Available online at www.sciencedirect.com

ScienceDirect

MATTER AND RADIATION AT EXTREMES

Matter and Radiation at Extremes 2 (2017) 16–21

www.journals.elsevier.com/matter-and-radiation-at-extremes

Research Article

Aluminum X-ray mass-ablation rate measurements

J.L. Kline [a,*], J.D. Hager [a,b]

[a] *Los Alamos National Laboratory, Los Alamos, NM 87545, USA*
[b] *Lockheed-Martin, Syracuse, NY 13221, USA*

Received 16 August 2016; revised 11 September 2016; accepted 18 September 2016
Available online 15 October 2016

Abstract

Measurements of the mass ablation rate of aluminum (Al) have been completed at the Omega Laser Facility. These measurements show that the mass-ablation rate of Al is higher than plastic (CH), comparable to high density carbon (HDC), and lower than beryllium. The mass-ablation rate is consistent with predictions using a 1D Lagrangian code, Helios. The results suggest Al capsules have a reasonable ablation pressure even with a higher albedo than beryllium or carbon ablators and further investigation into the viability of Al capsules for ignition should be pursued.
Copyright © 2016 Science and Technology Information Center, China Academy of Engineering Physics. Production and hosting by Elsevier B.V. This is an open access article under the CC BY-NC-ND license (http://creativecommons.org/licenses/by-nc-nd/4.0/).

PACS codes: 52.57.-z; 52.57.Fg; 52.57.Bc

Keywords: Inertial confinement fusion ablator; Aluminum ablator; Aluminum capsule; X-ray mass ablation rate; Alternate ablator

1. Introduction

For indirect drive inertial confinement fusion (ICF) [1], each ablator material has properties that provide unique advantages and disadvantages for ignition designs. For instance, the high mass ablation rate of beryllium capsules provides better stabilization for hydrodynamic instabilities at the ablation front and enables lower radiation temperature designs than that of carbon based ablators. High Density Carbon (HDC) ablators have high density, allowing thinner capsules with short laser pulses. For indirect drive, shorter laser pulses reduce the time-dependent effects of the hohlraum drive, leading to better control of the implosion symmetry. Plastic (CH) ablators are easy to make and can be doped with many mid to high Z materials to address gold M-band preheat from hohlraum radiation, and can also be effectively used to diagnose implosion performance. Another potential ablator material is aluminum (Al). Al has properties that make it a potential choice for capsule implosions. Al capsules provide a single species ablator and require no buried interfaces to block gold M-band preheat since the mean free path in this frequency range is ~3 μm, a factor of 6 better than high density carbon and a factor of >21 better than plastic (CH). Al may also be more stable to Richtmyer–Meshkov instabilities due to the impedance mismatch, reducing the shock strength across the boundary [2]. While Al's mass-ablation rate is expected to be comparable to that of other ICF ablator materials, it has not been measured; and since Al is a high *Z* material, the effect of a higher albedo and shielding by the blow-off could negate this assertion. For these reasons, it is useful to determine whether the effort needed to manufacture Al capsules is warranted and the mass-ablation rate is one metric. In addition, Al is often used as a standard baseline material to provide a relative comparison with other materials in many Equation of State (EOS) experiments. Thus, capsule implosion comparisons among different materials could use Al capsules as a baseline for implosion performance to normalize EOS effects.

* Corresponding author.
E-mail address: jkline@lanl.gov (J.L. Kline).
Peer review under responsibility of Science and Technology Information Center, China Academy of Engineering Physics.

http://dx.doi.org/10.1016/j.mre.2016.09.003
2468-080X/Copyright © 2016 Science and Technology Information Center, China Academy of Engineering Physics. Production and hosting by Elsevier B.V. This is an open access article under the CC BY-NC-ND license (http://creativecommons.org/licenses/by-nc-nd/4.0/).

To benchmark the performance of Al as an ablator, the mass-ablation rates of sputtered aluminum foils are measured. This provides insight into the ablation pressure p_a for the material, which is proportional to the material sound speed c_s at the ablation front multiplied by the mass ablation rate $\dot{m}$, i.e., $p_a \propto \dot{m} c_s$. The mass-ablation rate is also an important parameter for evaluating the rocket efficiency and ablation front hydrodynamic stability. Measurements of the Al mass-ablation rate as a function of the radiation temperature between 180 and 250 eV suggest Al is worth pursing as capsule ablators. The measured mass-ablation rate coefficient is slightly higher than that for HDC, although it is within the measurement error. The mass ablation measurements and a discussion in the context of other capsule ablator materials are presented in this manuscript.

2. Experimental setup

The X-ray mass-ablation rate is determined from a measurement of the differential burn-through time of two aluminum foils, with a known difference in thickness, driven by the X-ray produced by a gold half-hohlraum. The technique was developed by Olson et al. [3] at the Omega Laser Facility [4,5]. A detailed experimental description can be found in Ref. [3]. For the mass-ablation measurement, two sample foils with different thicknesses are attached to the back of a gold half-hohlraum as shown in Fig. 1. The half-hohlraum is aligned along a pentagonal axis (P6-P7) of the Omega laser system which provides azimuthally symmetric illumination of the half-hohlraum by 15 drive beams splitted into two cones, one with 10 beams and the other with 5 beams. The two foils are then irradiated by the nearly Planckian drive of the hohlraum. An imaging streak camera with a transmission grating snout positioned to record X-rays at ~700 eV is pointed at the backside of the hohlraum with the two foils. As the foils burn-through, each foil becomes transparent to the 700 eV X-rays from the half-hohlraum. The selection of 700 eV photons for the differential burn-through is arbitrary between 400 eV and 800 eV and done here for consistency with Olson et al. While measuring the differential burn-through with different energy photons will shift the absolute time, it doesn't affect the differential burn-through time. From the streak camera data, the

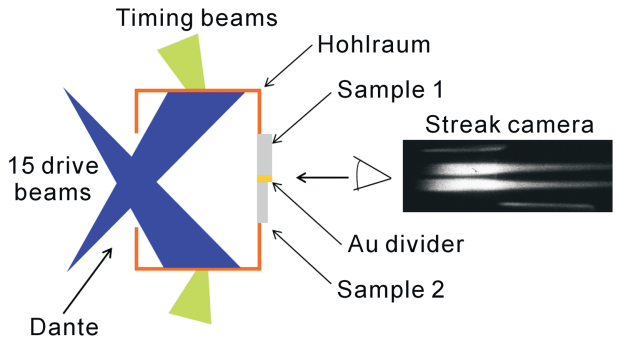

Fig. 1. Experimental layout showing the drive beams, the timing beams, the gold hohlraum, the sample foils, along with the locations of the diagnostics. The inset image for the streak camera shows typical data with the timing beams at the top and bottom and the X-ray burn-through of the two foils.

difference in burn-through time for the two foils can be determined. From the measured foil density, differential thickness and differential burn-through time, the X-ray mass-ablation rate can be determined using

$$\dot{m} = n\Delta x/\Delta t, \tag{1}$$

where $\dot{m}$ is the mass-ablation rate, n is the density, Δx is the differential thickness of the two foils, and Δt is the differential burn-through time.

To produce a range of different radiation temperatures, three different gold hohlraums combined with three laser pulses are used. Fig. 2(a) shows schematics of the three hohlraums ranging from scale 1 Omega with a 1600 μm diameter, a 1200 μm length, and a 1200 μm diameter Laser Entrance Hole (LEH) to a 5/8 scale with a 1000 μm diameter, a 750 μm length and a 800 μm diameter LEH. All of the hohlraums have a 650 μm diameter hole on the rear wall of the half-hohlraum to view the foils and measure the radiation as it passes through. Each foil is mounted over half of the rear exit hole with a gold divider as shown in Fig. 2(a). In addition to the different hohlraum sizes, three different laser pulse shapes with different energies are used to generate different drive temperatures. The highest radiation temperatures are produced with the 1 ns square pulse in the 5/8 and 3/4 scale hohlraums. For intermediate radiation temperatures, the reversed ramp pulse shape is used at two different laser energies, and the low radiation temperature uses the scale 1 hohlraum with the 2 ns square pulse (see Fig. 2(b)). The corresponding X-ray drive histories measured with the Omega Dante [6,7] for the five configurations are shown in Fig. 2(c). The Dante diagnostic uses a combination of K- and L-edge filters and X-ray diodes to measure the flux at different energies emanating from the LEH of the half-hohlraum. The line colors in Fig. 2(c) correspond to the laser pulses with the same color and the line styles correspond to the half-hohlraum scales. An example spectrum from a Dante unfold along with the equivalent Planckian spectrum at 256 eV corresponding to a 5/8 scale hohlraum with 1 ns square pulse is shown in Fig. 3. The spectral unfold method for analyzing the Omega Dante data uses an archaic algorithm [8,9] that introduces features in the spectrum as a result of the waveforms used to represent the response functions for each channel. The amplitude of the response function for each channel is varied to match the measured voltages for each channel. These features can be unphysical either as a result of Dante component calibration or due to X-ray transition radiation, but it is challenging to determine which way it is since the unfold is an inverse problem. However, the total flux determined from the unfolded spectrum is typically within a few percent of more advanced algorithms since the interplay between the response and the measurement of each channel tends to compensate for variations in the channel calibrations [10–12]. In Fig. 3, there is a peak larger than the related Planckian, but the spectrum falls below at higher photon energies leading to a total flux measurement that is comparable to a Planckian of the same color temperature as the Dante unfolded brightness temperature. Thus, the brightness

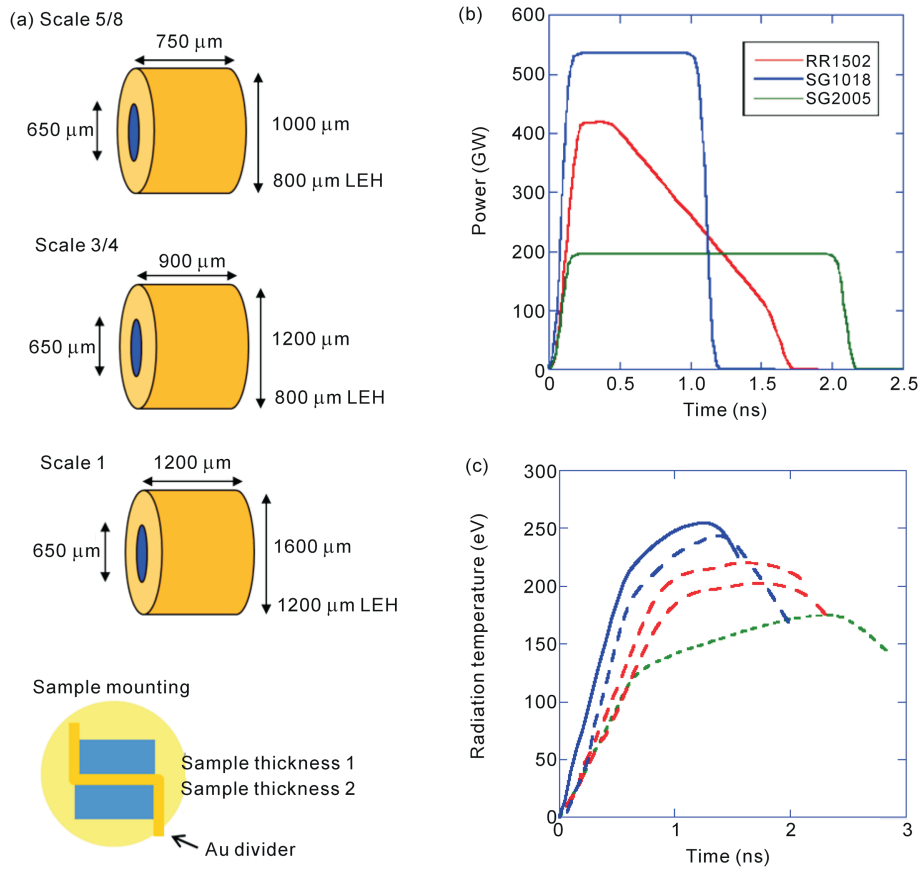

Fig. 2. (a) Schematics of the three hohlraum sizes with a diagram of the foil placement on the rear of the hohlraums along with the Laser Entrance Hole (LEH) size. (b) The three laser pulse shapes used to drive the hohlraums. (c) The radiation temperature time histories for the five hohlraum/laser pulse shape combinations. The line color corresponds to that of the laser pulse shape above. The line style corresponds to the 5/8 (——), 3/4 (- - -) and 1 (···) hohlraum scale. Note, the two different temperature profiles for the reversed ramp with the 3/4 scale hohlraum are achieved by reducing the laser energy/beam from 500 J to 300 J.

temperature, which includes the gold M-band component, is accurate to ~2.5%. While there has been work to improve the spectral unfold from Dante like spectrometers, it has focused on recovering a more accurate spectrum [13,14].

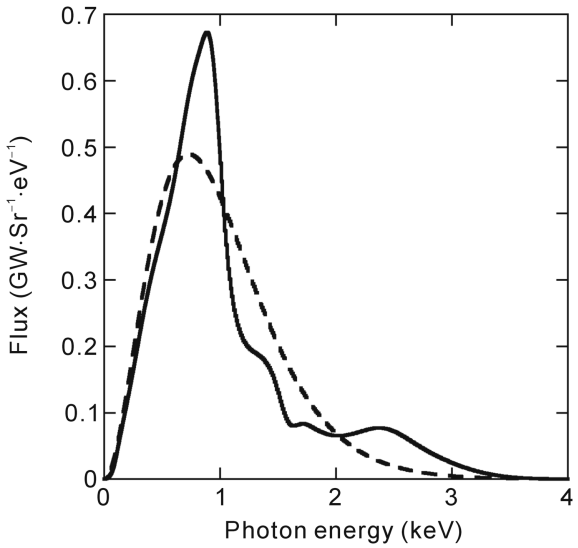

Fig. 3. Dante unfolded spectrum (——) with the equivalent Planckain spectrum (- - -) for a radiation temperature of (258 ± 6) eV for a 5/8 scale hohlraum with a 1 ns square pulse (solid blue curve in Fig. 2).

To relate the mass-ablation rate to the X-ray radiation temperature, the time at which the burn-through occurs must be correlated to the drive temperature of the half-hohlraum measure by the Dante [6,7]. To both determine the exact time of the burn-through relative to the Dante and to calibrate the time axis of the streak camera, two laser beams are pointed to the outside of the hohlraum on the top and bottom respectively. The beams provide two timing fiducials. Using the relative timing between the two timing fiducials and the main drive beams, the burn-through time can be related to the drive temperature. One important aspect to reduce the uncertainty in the drive is to keep the differential burn-through time to ~80 ps to minimize the change in the radiation temperature over the differential burn-through time. The error in the hohlraum temperature measurement with respect to the burn-through is determined by cross comparing the burn-through time with the Dante temperature history. The Dante temperature is taken at the center of the burn-through interval. The error, or range, for the Dante temperatures is taken as 1/2 of the burn width from the central point within ±50 ps. The additional 50 ps error on both sides of this range is due to the relative timing of the Dante temperature history with the incident and timing laser pulses.

The toughest challenge for these experiments is determining the foil thickness. To produce self-consistent data, sputtered Al foils are used because standard role aluminum foils have spatially dependent thickness variations that are

challenging to characterize. The sputtered foils are generated and characterized at Los Alamos National Laboratory (LANL). The sputtered Al foil density is measured using Rutherford backscattering and found to be 93% of the density of standard Al, i.e., (2.51 ± 0.13) g/cm^3 v.s. 2.70 g/cm^3. The advantage of the sputtered foils is that even the error in the absolute density may lead to a systematic measurement difference, the foil-to-foil variations are small. The foils for the experiments by Olson et al. were characterized by using a special *in situ* interferometry system after the targets were built [3]. However, for these experiments the described system was unavailable. The differential foil thickness was measured by using X-ray transmission with the LANL Density Characterization Station (DCS) [15]. The DCS is a monochromatic X-ray radiography source with a chromium source at 5.415 keV. To minimize the absolute error between the foil thicknesses, the X-ray transmission is measured for both foils *in situ* after mounting to the target. This increases the precision of the measurement of the difference in the foil thicknesses.

The differential burn-through time is determined from the streak records of the emission at 700 eV on the streak camera. The entire emission is spatially integrated and plotted versus time. Fig. 4 shows typical line outs for the X-ray burn-through, as well as X-rays generated by the laser beams pointed to the outer wall of the hohlraum at the top and bottom. The timing fiducials are used for cross-timing with the Dante and to provide a temporal calibration since Omega measures the absolute timing of each beam. The differential time is taken at 10% of the peak as by Olson et al. The idea is to take the earliest distinguishable time to minimize the experimental evolution for data set for consistency. However, one can see that the differential burn-through time is the same up to 30%–40% of the peak. The streak record is calibrated using the two fiducial pulses to provide the time-per-pixel for the differential burn-through. For the 4 ns streak sweep speed, the temporal resolution per pixel is ~3.68 ps. Since we are measuring the profiles across several pixels, the ability to obtain the time between the burn-through can be at the sub-pixel level.

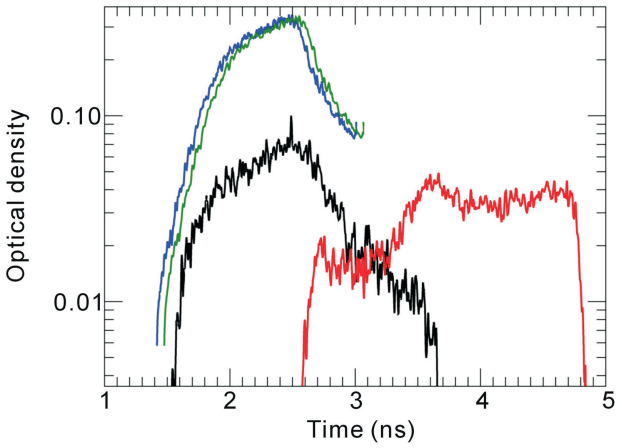

Fig. 4. Typical line outs showing different burn-through time in blue and green and the timing of the X-ray fiducals from the lasers pointed to the top and bottom outer wall of the hohlraum.

However, due to noise on the signals, the error in the differential time is close to 5 ps.

The measurement error for the mass-ablation rate, $\delta\dot{m}$, is given by the Taylor expansion of

$$\delta\dot{m} = \sqrt{\left[\left(\frac{\Delta x}{\Delta t}\right)\delta n\right]^2 + \left[\left(\frac{n}{\Delta t}\right)\delta\Delta x\right]^2 + \left[\left(\frac{n\Delta x}{(\Delta t)^2}\right)\delta\Delta t\right]^2} \quad (2)$$

where the δs are the measurement errors for the given quantities. Using this equation and the estimated individual error for each parameter for each measurement, the error is determined for every measurement of the X-ray mass-ablation rate.

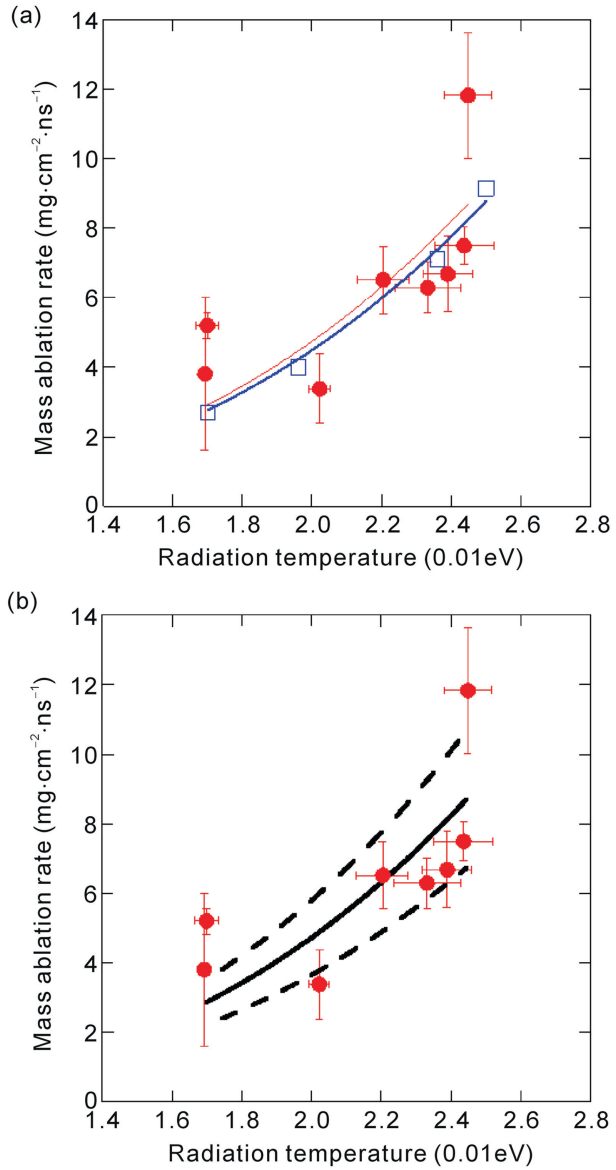

Fig. 5. (a) Measured aluminum mass-ablation rates (●) along with the predicted mass-ablation rate from Helios (□). The solid lines represent the fits with the measured ablation rate coefficient being (0.59 ± 0.6) mg·cm^{-2}·ns^{-1} and the predicted value being 0.56 mg·cm^{-2}·ns^{-1}; (b) A comparison of the measured aluminum mass-ablation rate with the fitted data (——) along with the confidence intervals for the fit (- - -).

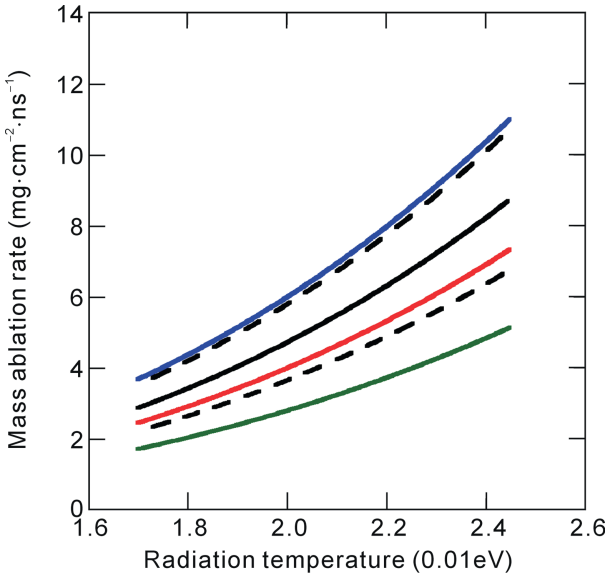

Fig. 6. Comparison of the fit to the measured Al mass-ablation rate (——) along with the confidence intervals (- - -) to that of beryllium (——), high density carbon (——) and Ge doped CH (——).

For these experiments, the dominant error is the measurement of the foil thickness.

3. Measurements of the aluminum mass-ablation rate

Measurements of the aluminum mass-ablation rate are shown in Fig. 5(a) as a function of radiation temperature. The solid red curve is a fit to the equation $\dot{m} = aT^3$ since the ablation rate has a T^3 dependence where T is the hohlraum radiation temperature and is derived in the manuscript by Lindl [1]. Here a is the ablation rate coefficient. The fit gives a value of (0.59 ± 0.06) mg·cm^{-2}·ns^{-1} (0.01eV)$^{-3}$ for the Al mass-ablation rate coefficient. The error is the 1σ standard fitting error for the data. The blue squares on the curve are those calculated by the 1D Helios CR radiation hydrodynamics code [16]. For the simulations, the radiation temperatures from the Dante measurements are used as a source to drive the Al foils with varying absolute thickness, but the same differential thickness and a density of 2.51 g/cm^3. The breakout time is determined from the radiation passing through the Al foil at ~700 eV to mimic the experiments. The ablation coefficient predicted by simulations is 0.56 mg·cm^{-2}·ns^{-1} (0.01eV)$^{-3}$. Thus, the experimental measurements and calculated values are in good agreement. Fig. 5(b) shows the data with the aT^3 fit plus the 95% confidence intervals. The large fit error and confidence intervals are driven by the outliers at 1.7 and 2.4 (0.01eV). While these points appear to be outliers, there is no viable reason to remove them from the data set. It should be noted that the T^3 dependence assumes the ionization state and the albedo remain approximately the same. The peak of the Planckian drives at 170 eV and 250 eV have the peak photon energies of ~5 times above the Al L-shell and ~2 times below the Al K-shell. The point at 240 eV jumps well above the other data and is believed to be an experimental outlier. However, on the lower end of the temperature range, the assumptions may break down since both data points are above the fit even though one is within the experimental error. Without these points, the error is greatly reduced along with the confidence intervals.

Fig. 6 shows a comparison of the mass-ablation rate for Al to that of beryllium, HDC, and Ge doped CH [3]. The value of the ablation coefficient of 0.59 is slightly higher than that of HDC at 0.5, but HDC is within the measurement error. If the point at 11.8 mg·cm^{-2}·ns^{-1} is removed the fit coefficient lowers to 0.53 but HDC is still within the measurement error. Al is clearly better than plastic (CH) at 0.35 and below that of beryllium which is outside the confidence interval with an ablation rate coefficient of 0.75.

4. Conclusions

The mass-ablation rate for sputtered aluminum has been measured using the same technique as for other ICF ablator materials at the Omega laser. When compared with other lower Z ablator materials, aluminum appears to have a favorable mass-ablation rate. The value of its ablation coefficient of 0.59 is slightly higher than that of HDC, although HDC is within the measurement error. The ablation coefficient value of Al is between that of plastic (CH) and beryllium. With the given mass-ablation rate, the ablation pressure from Al should be comparable to HDC, although the higher Z of Al will reduce the sound speed by the order of 10% for radiation temperatures in the 300 eV range, since it will mostly be in the hydrogen-like state. Overall, the data suggest that Al would be a reasonable choice for an ICF ablator.

Acknowledgements

We wish to thank Derek Schmitt and Deanna Capelli for target fabrication and Igor Usov for generating and characterizing the sputtered Al foils. We would also like to thank Joe Cowan for the X-ray transmission measurements. We thank Rick Olson for many useful discussions of his experimental design and providing the initial target drawings created at Sandia National Laboratory and Steve Batha for scientific and editorial comments on the manuscript. This work is performed under the auspices of the U.S. Department of Energy by LANL undercontract DE-AC52-06NA25396.

References

[1] J. Lindl, Development of the indirect-drive approach to inertial confinement fusion and the target physics basis for ignition and gain, Phys. Plasmas 2 (1995) 3933–4024.
[2] P. Amendt, Personal Communication (2014).
[3] R.E. Olson, G.A. Rochau, O.L. Landen, R.J. Leeper, X-ray ablation rates in inertial confinement fusion capsule materials, Phys. Plasmas 18 (2011) 032706.
[4] T.R. Boehly, R.S. Craxton, T.H. Hinterman, J.H. Kelly, T.J. Kessler, et al., The upgrade to the Omega laser system, Rev. Sci. Instrum. 66 (1995) 508–510.
[5] J.M. Soures, R.L. McCrory, C.P. Verdon, A. Babushkin, R.E. Bahr, et al., Direct-drive laser-fusion experiments with the OMEGA, 60-beam, >40 kJ, ultraviolet laser system, Phys. Plasmas 3 (1996) 2108–2112.

[6] H.N. Kornblum, R.L. Kauffman, J.A. Smith, Measurement of 0.1−3-keV X rays from laser plasmas, Rev. Sci. Instrum. 57 (1986) 2179−2181.
[7] C. Sorce, J. Schein, F. Weber, K. Widmann, K. Campbell, et al., Soft X-ray power diagnostic improvements at the Omega Laser Facility, Rev. Sci. Instrum. 77 (2006) 10E518.
[8] H.F. Finn, UNSPEC Reference Manual Version 10/29/82, 1982.
[9] R.L. Kauffman, H.N. Kornblum, D.W. Phillion, C.B. Darrow, Drive characterization of indirect drive targets on the Nova laser (invited), Rev. Sci. Instrum. 66 (1995) 678−682.
[10] A. Seifte, G.A. Kyrala, Different methods of reconstructing spectra from filtered X-ray diode measurements, Rev. Sci. Instrum. 79 (2008) 10F323.
[11] D.L. Fehl, F. Biggs, Verification of unfold error estimates in the unfold operator code, Rev. Sci. Instrum. 68 (1997) 890−893.
[12] M.J. May, K. Widmann, C. Sorce, H.S. Park, M. Schneider, et al., Uncertainty analysis technique for OMEGA Dante measurements, Rev. Sci. Instrum. 81 (2010) 10E505.
[13] J. Li, X.B. Huang, S.Q. Zhang, L.B. Yang, W.P. Xie, et al., Investigation of spectra unfolded for a filtered X-ray diode array with improved smoothness, Rev. Sci. Instrum. 80 (2009) 063106.
[14] R.E. Marrs, K. Widmann, G.V. Brown, R.F. Heeter, S.A. Maclaren, et al., Use of a priori spectral information in the measurement of X-ray flux with filtered diode arrays, Rev. Sci. Instrum. 86 (2015) 103511.
[15] N.E. Lanier, C. Hamilton, J.M. Taccetti, A monochromatic X-ray imaging system for characterizing low-density foams, Rev. Sci. Instrum. 83 (2012) 10E521.
[16] J.J. Macfarlane, I.E. Golovkin, P.R. Woodruff, HELIOS-CR A 1-D radiation-magnetohydrodynamics code with inline atomic kinetics modeling, J. Quant Spectrosc. Radiat. Transf. 99 (2006) 381−397.